Microgravity Science and Technology (2018) 30:817–829
https://doi.org/10.1007/s12217-018-9624-7

ORIGINAL ARTICLE

# Laser Interferometer for Space Gravitational Waves Detection and Earth Gravity Mapping

**Yuqiong Li[1] · Ziren Luo[1] · Heshan Liu[1] · Ruihong Gao[1,2] · Gang Jin[1]**

Received: 4 December 2017 / Accepted: 8 May 2018 / Published online: 19 June 2018


**Abstract**
The idea of using space laser interferometer to measure the relative displacement change between two satellites has been considered for space gravitational waves detection and Earth gravity filed mapping in recent years. Some investigations on the key issues of laser interferometer in our working team have been presented in this paper. An on-ground laser interferometer prototype used for the demonstration of satellite-to-satellite ranging has been constructed, which is equipped with phasemeter, laser pointing modulation and laser phase-locking control. The experimental results show that path-length measurement sensitivity of the laser interferometer reaches 200 pm/$\sqrt{}$Hz, and phase measurement precision achieves $2\pi \times 10^{-5}$ rad/$\sqrt{}$Hz, and laser pointing modulation precision is better than 80 nrad/$\sqrt{}$Hz, and laser phase-locking control precision attains $2\pi \times 10^{-4}$ rad/$\sqrt{}$Hz within the frequency regime of 1 mHz–1 Hz. All of these demonstrate that the proposed laser interferometer has very promising feasibility to meet the requirement of the Taiji, TianQin and Space Advanced Gravity Measurement (SAGM) missions which are put forward by Chinese scientists.

**Keywords** Laser interferometer · Gravitational waves · Earth gravity filed

## Introduction

Laser interferometer is widely used in various gravitational waves detectors, including the Laser Interferometer Gravitational-Wave Observatory (LIGO) in the United States, evolved Laser Interferometer Space Antenna (eLISA) in European Space Agency, and DECi-hertz Interferometer Gravitational Wave Observatory (DECIGO) in Japan. The LIGO has observed gravitational waves from the merger of two stellar-mass black holes (Abbott et al. 2016a, b, 2017) which is the first direct detection of gravitational waves and the first observation of a binary black hole merger. In 2016, a space gravitational waves detection mission called Taiji was put forward by the Chinese Academy of Sciences (Cyranoski 2016), which would consist of a triangle of three spacecraft in orbit around the Sun. The Taiji's spacecraft would be separated by 3 million kilometers, and the required measurement sensitivity of laser interferometer would be 10 pm/$\sqrt{}$Hz within the frequency range of 0.1 mHz–1 Hz (Gong et al. 2011; Li et al. 2012; Cyranoski 2016). A second Chinese proposal called TianQin led by the Sun Yat-Sen University, which has three satellites that orbit Earth at a distance of about 150,000 kilometers from each other. This mainly target a particular pair of orbiting white dwarf stars, called HM Cancri (Cyranoski 2016).

The information gained about the global gravity field from the Gravity Recovery and Climate Experiment (GRACE) raised an interest in developing a follow-on mission with better temporal and spatial resolution. Besides the microwave inter-satellite ranging metrology system, the GRACE follow-on mission will carry a satellite-to-satellite laser interferometer for demonstrating the feasibility of long baseline space laser interferometer and improving the distance measurement precision between two satellites, which will be launched in 2018 (Bender et al. 2003; Nagano et al. 2005; Pierce et al. 2008; Lhermite et al. 2007; Sheard

This article belongs to the Topical Collection: Approaching the Chinese Space Station - Microgravity Research in China
Guest Editors: Jian-Fu Zhao, Shuang-Feng Wang

✉ Gang Jin
gajin@imech.ac.cn

[1] National Microgravity Laboratory, Institute of Mechanics, Chinese Academy of Sciences, Beijing 100190, China

[2] School of Engineering Science, University of Chinese Academy of Science, Beijing 100049, China

et al. 2012; Heinzel 2017; Olivier et al. 2014). The SAGM is designed for the Earth's gravity recovery mission proposed in China, which will greatly improve the temporal-spatial resolution of the Earth's gravity. The required inter-satellite distance and range accuracy for the SAGM is 200 km and 10 nm/$\sqrt{}$Hz at 0.1 Hz, respectively (Yeh et al. 2011).

The key techniques for space laser interferometer ranging system include high frequency stability laser, high precision phase-meter, laser phase-locking control, high stability laser pointing modulation, arm-locking, time delay interferometer and so on (Danzmann and LISA Study Team 1996; Nagano et al. 2004; Heinzel et al. 2006; Dehne et al. 2009; Bender et al. 2013). From the measurement principle of space borne laser interferometer can be known that an ultra-stable laser interferometer optical bench should be prepared to make the reference beam and measurement beam produce an interference signal, then the phase information of which will be detected by a phasemeter to derive the displacement information between the satellites. For the satellites in space will suffer from solar wind, cosmic rays, interstellar magnetic field, etc. non-conservative forces, the laser beam will jitter resulting in a phase noise due to the geometrical distortion of the receiving telescope. So, a laser beam pointing control system is needed to suppress the jitter of transmitting light. Meanwhile, for the satellites are separated by millions of kilometers in Taiji mission, the laser beam from the remote spacecraft arrives at the local spacecraft will become very weak (about 100 pW), a laser phase-locking control used for phase locking and light amplification is necessary. Therefore, our working team has developed some key technologies such as high precision phasemeter, high sensitivity laser interferometer, high precision laser pointing modulation, and high precision laser phase-locking control. The progress on these key technologies will be presented in the paper.

## Key Technologies

### High Precision Digital Phasemeter Prototype

#### Design and Architecture

Various types of phase measurement techniques have been considered for the gravitational waves detection and gravity field measurement. Liang et al. (2012) reported that they had developed a phasemeter based on cross-correlation and obtained a noise level of $1.2 \times 10^{-6}$ rad/$\sqrt{}$Hz@1 Hz. But this phase measurement method is limited by the fixed frequency input, which is not suitable for the Doppler shift in the satellite-to-satellite tracking. While the most suitable phasemeter architecture, which can provide the required accuracy for the Taiji and SAGM missions, is based on a scheme called digital phase-locked loop (DPLL) (Heinzel et al. 2004; Bykov et al. 2009). The Albert Einstein Institute (AEI), Germany and Jet Propulsion Laboratory (JPL), America reported that they had developed some phasemeter prototypes of phase readout precision up to $2\pi$ $\mu$rad/$\sqrt{}$Hz in the frequency band from 0.1 mHz to 10 Hz (Shaddock et al. 2006; Gerberding et al. 2013). A digital phasemeter with multi-channel, which is built upon field programmable gate array (FPGA, DE3-340, Terasic) and based on DPLL scheme, has been developed by our group team. The schematic of the multi-channel phasemeter is shown in Fig. 1. The detected signals are modulated and digitized by the analog to digital converter (ADC, AD9254) board, then enter into the FPGA for realizing the DPLL algorithm. Firstly the ADC board needs to be aroused by the relevant driver program, then the digitized signals are respectively multiplied by the numerically controlled oscillator (NCO) with sine and cosine signals in the same frequency. After that, the multiplied frequency parts are filtered by two low pass filters (LPF). The remained value after filtering is proportion to the related phase difference between the detected signal and the NCO. Lastly, four series of phase data are exported for further analysis. For decreasing the phase noise caused by the integration of frequency error, the multi-channel phasemeter developed here introduces only one feedback loop, and the frequency of NCOs between channels are changed synchronously, as shown in Fig. 1b. So, the multi-channel phasemeter developed here is mainly used in the ground interferometer demonstration, the frequency fluctuations between interferometer arms of which can be neglected. In the phasemeter prototype, all parts are synchronized by one oscillator for reducing the clock noise.

#### Experimental Results and Discussions

The physical picture of the phasemeter is show in Fig. 2. Here the performance of the phasemeter was evaluated under the condition that the tested signal was generated by a functional generator (33522A, Agilent), and the data were analyzed with a method called linearization amplitude spectral density (LASD), the toolbox of which was developed by the Max Planck Institute for Gravitational Physics. The frequency and amplitude of the tested signal is 1 MHz and 100 mV, respectively. For decreasing the influence of phase error between different signals, one signal from the functional generator is split into four, then they are input into the four channels (named A, B, C and D, A and B share one ADC board, C and D share the other ADC board) of the phasemeter. Besides the measurement precision, the

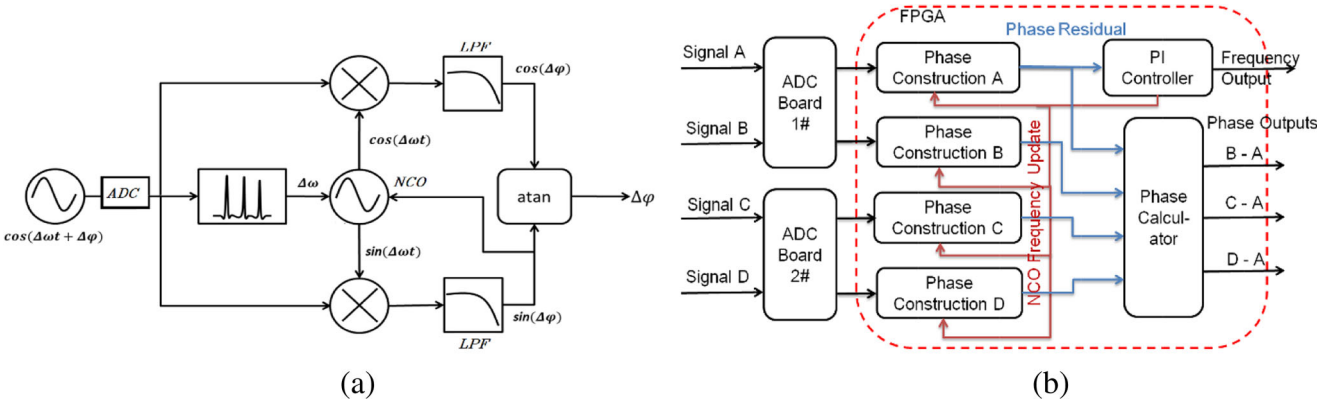


**Fig. 1** Schematic diagram of the phasemeter. **a** the detailed schematic diagram of one channel; **b** the whole schematic diagram of the multi-channel phasemeter

uniformity of the multi-channel response is also concerned in the experiment. The results are shown in Fig. 3.

From the results of Fig. 3 can be seen that the sensitivity of the phasemeter reaches $2\pi$ $\mu$rad/$\sqrt{}$Hz within the frequency range of 0.1 Hz–10 Hz. However, it is also noticed that there are some peaks appear inside the frequency regime of 3 Hz 10 Hz, and the peaks of red and green curves are higher than that of the blue curve. The peaks are the remained noise of the feedback, which appear in the place of the frequency multiplication of frequency difference between the detected signal and the NCO. Since the detected signals are the same for each channel of the phasemeter, the peaks should exist in all channels. Actually, the output of the phasemeter is the phase difference between channels, the peaks can be removed through the subtraction in principle. However, the output results are not the phases at the same moment for different channels having different time delay. So, the value of time difference between channels determines the peaks value. From the comparisons between the green, red and blue curves, it can be concluded that the effect of time difference on non-adjacent channels is very obvious. From Fig. 3, it can also be seen that the noise floor of different curves increase differently in the frequencies below 0.1 Hz. From the previous investigations (Liu et al. 2014), it could be deduced that the thermal drift is the main factor that influences the analog frontend of ADC. Besides, limited by the hardware condition, four ADCs and their analog frontends distribute on two different ADC boards, which leads the temperature fluctuations between different frontends to be large. Other noises including sampling jitter noise, quantization noise, feedback loop noise, etc. were analyzed in the previous investigations (Liu et al. 2014).

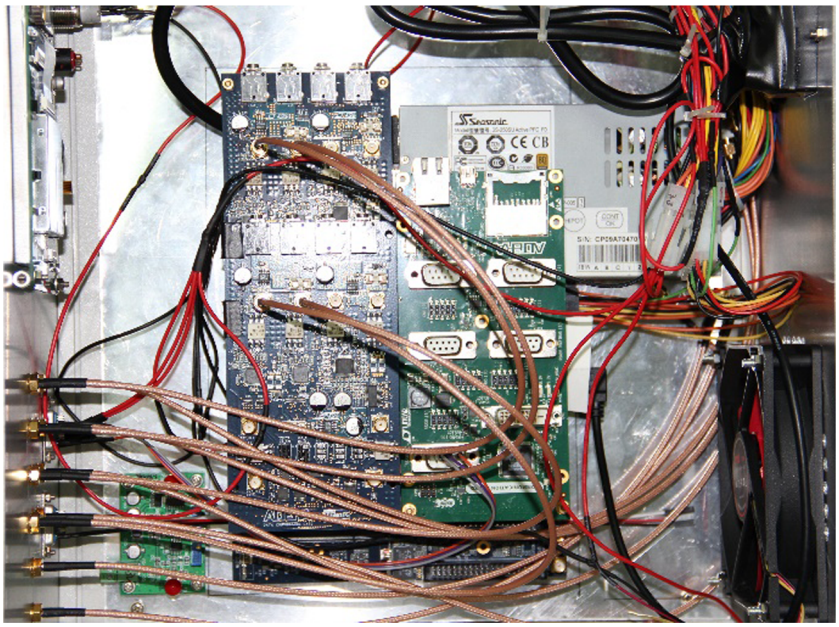

**Fig. 2** Physical picture of the phasemeter

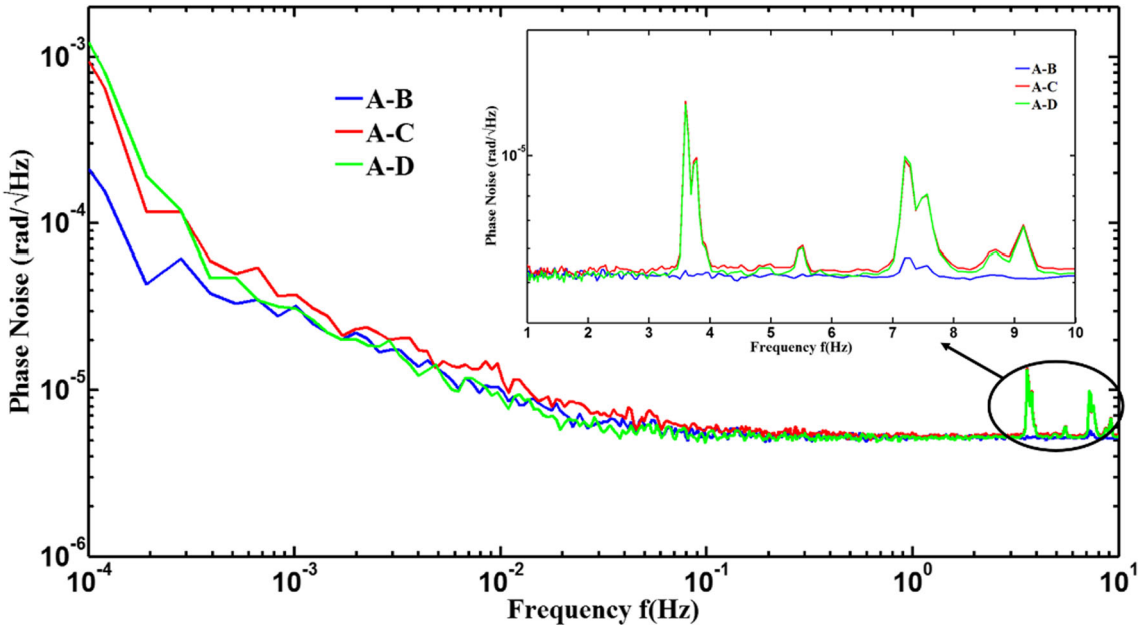


**Fig. 3** Phase noise of the phasemeter


## Summary

A multi-channel phasemeter which can parallelly process interference signals has been constructed. The results show that the precision of the phasemeter could achieve $2\pi$ $\mu$rad/$\sqrt{}$Hz in the frequency range of 0.1 Hz–10 Hz. Some peaks caused by the feedback loop appear in the non-adjacent channels' readout, and the thermal noise increases greatly in the frequencies below 0.1 Hz due to the different ADC boards. Customized board and thermal insulation methods will be adopted to decrease the effect in the future study. The prototype developed in this paper doesn't meet the requirement of the Taiji and SAGM missions to extract the length information, because the missions couldn't introduce a reference optical path. However, the prototype can be used for beam pointing mission ($\geq$four channels) and measuring the relative motion between the testmass and optical bench in the ground demonstration of laser interferometer. The process of identifying and removing noises to make the phasemeter meet the requirement of the Taiji and SAGM missions in our working team is being continued.


## Polarizing Laser Interferometer Prototype

Yeh et al. (2011) reported that a transponder-type intersatellite laser ranging system with 10-m baseline by using a homodyne optical phase locking technique was built up to demonstrate the validity of the measurement scheme, and a resolution of displacement measurement of about 3.2 nm had been achieved. In the previous investigations, an on-ground methodological demonstration of laser interferometer had been built (Li et al. 2012). In this paper, an on-ground polarizing laser interferometer prototype equipped with one reference interferometer and two measurement interferometers having equal-length arms has been constructed, the optical design of which is similar to that of LISA Pathfinder except for the adoption of polarizing light.

## Design and Architecture

To minimize the effects of thermal noise, electromagnetic noise and vibration noise on the ranging accuracy of the laser interferometer, an optical table with passive vibration isolation based on an isolated ground is adopted, on which a vacuum chamber is constructed (Sascha et al. 2017). The schematic diagram of the experimental setup and the physical picture of the laser interferometer prototype are shown in Figs. 4 and 5, respectively. The vibration isolation system consists of an isolated ground and a suspended optical table, the resonance frequency of which is about 1 Hz. During the pumping process of the vacuum chamber, three pumps are used: a rotary pump, a turbo pump and an ion pump. However, the rotary pump and turbo pump would cause vibration noise while the ion pump would bring thermal noise and electromagnetic noise. Thus, all the three pumps were all stopped after the pressure of the vacuum chamber reached $2 \times 10^{-6}$ mbar, and thus the pressure may rise to about $10^{-3}$ mbar when the path-length fluctuations are being measured, which could take about 72 h.

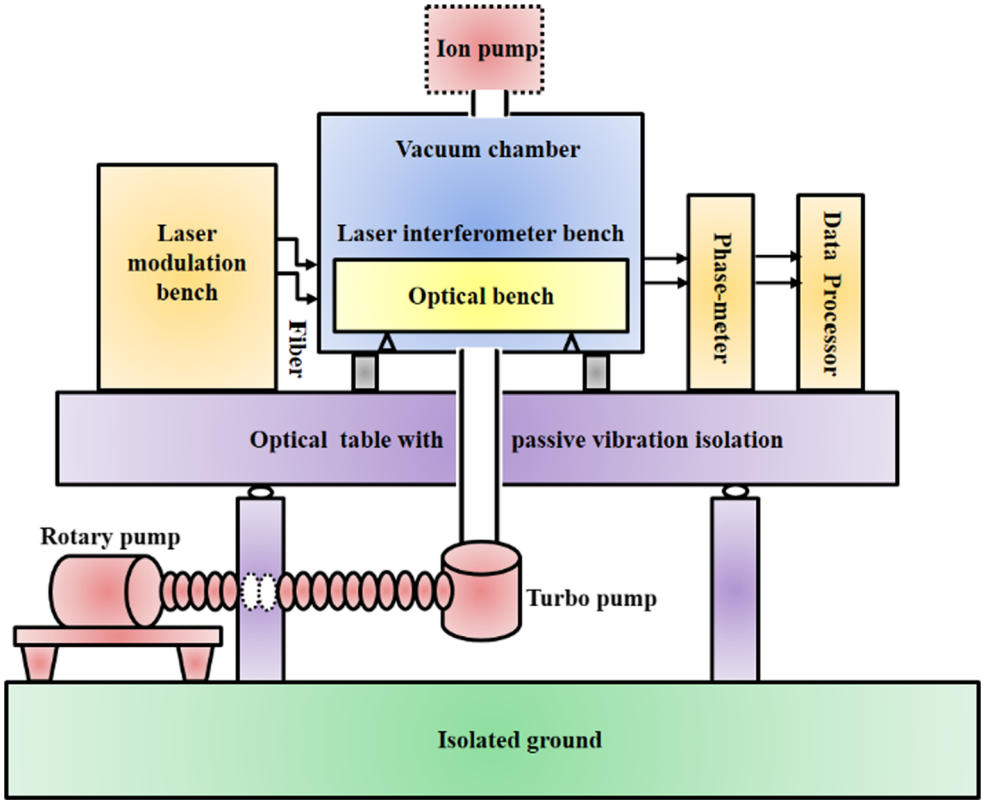


**Fig. 4** Schematic diagram of the experimental setup

As a polarizing layout is convenient to separate ingoing and returning beams, here the proposed optical design adopts such a polarizing layout. The laser interferometer layout consists of a modulation bench and an optical bench, the schematic diagram of which is shown in Fig. 6.

The modulation bench located outside of the vacuum chamber, which provides laser beam preparation. The linearly polarized light emitted from the laser (made in Beijing, wavelength $\lambda = 1064$ nm, power $P = 300$ mW, frequency instability $\Delta f = 1$ MHz/2 h) passes through a

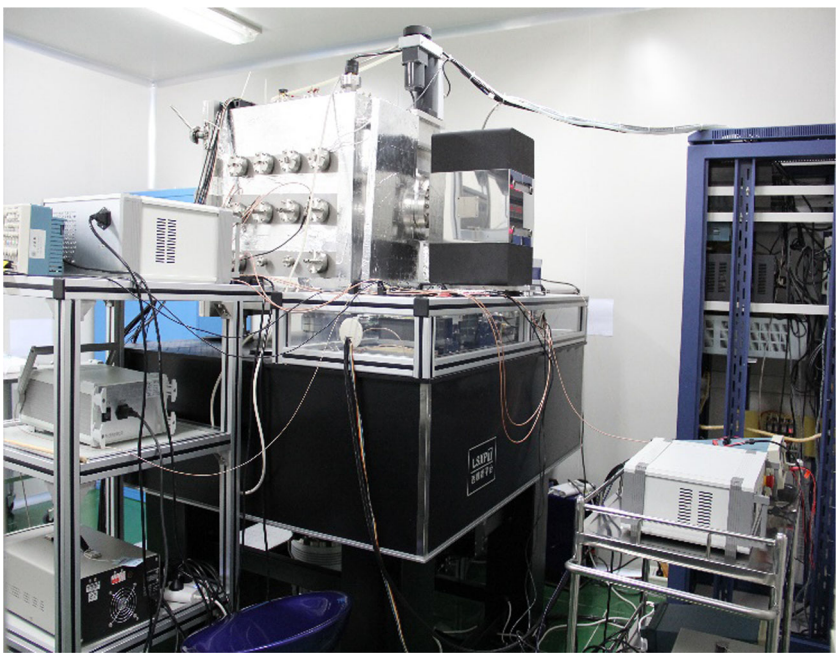

**Fig. 5** Physical picture of the laser interferometer prototype

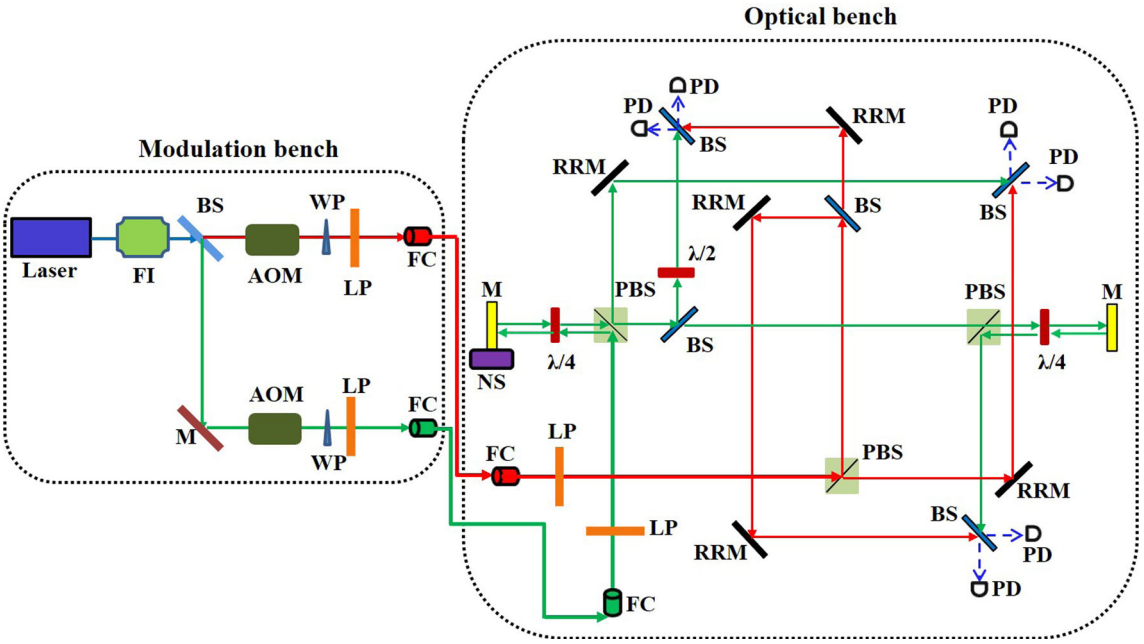


**Fig. 6** Schematic diagram of the heterodyne interferometer. FI: Faraday Isolator, BS: 50/50 Beam Splitter, M: Mirror, AOM: Acousto-optic Modulator, WP: Wedged Plate, LP: Linear Polarizer, FC: Fiber Coupler, RRM: Rectangular Reflection Mirror, PBS: Polarizing Beam Splitter, PD: Photo-detector, NS: Nanopositioning Stage

Faraday isolator to avoid back-reflection of the laser beam. Then, the laser frequency is modulated by using AOMs at approximately 70 MHz with a frequency difference $f_{\text{het}}$ of 1 MHz, the relative frequency instability of which is $10^{-7}$. Finally, the frequency-shifted beams are injected into the optical bench in the vacuum chamber by two single-mode optical fibers. The role of the wedged plate is to make the laser beam emitted from the AOM's first diffraction become parallel to the optical bench.

The optical bench located in the vacuum chamber contains one reference interferometer and two measurement interferometers, performing the path-length fluctuations measurement. Figure 7 shows the physical picture of the optical bench. The reference interferometer senses the common-mode phase fluctuations caused by the environmental noises, such as mechanical and thermal fluctuations, which occur outside the stable optical bench, as shown in Fig. 8a. The testmass-bench measurement interferometer

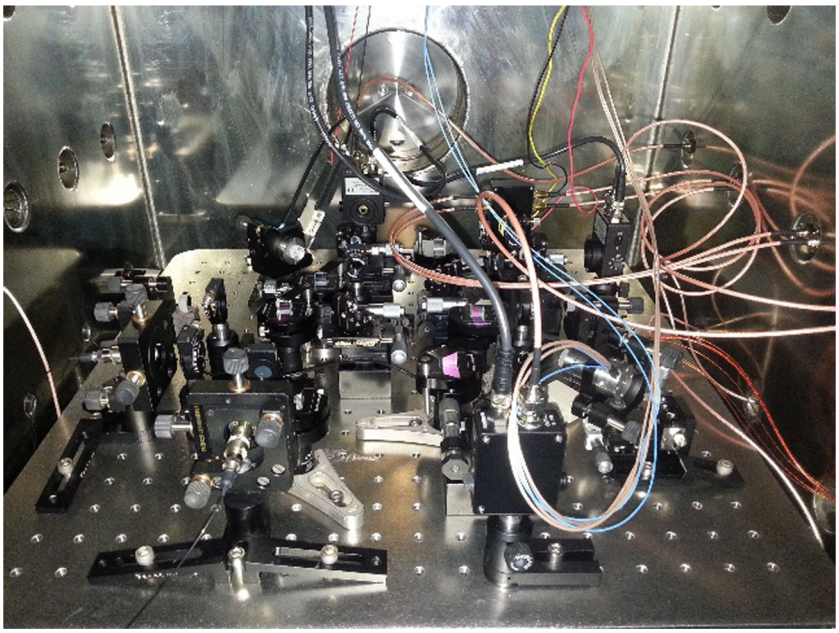

**Fig. 7** Physical picture of the optical bench

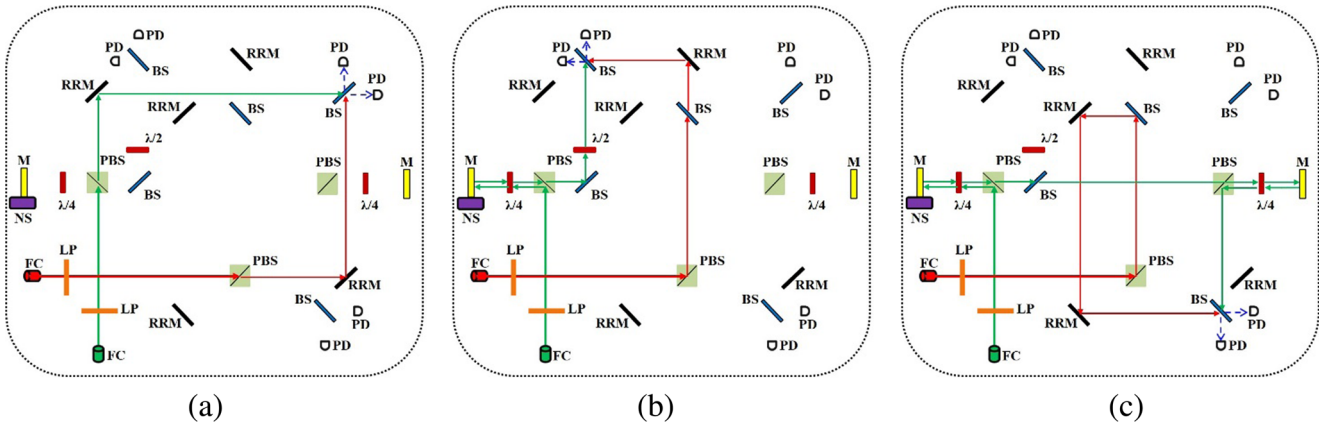


**Fig. 8** Schematic diagram of the three interferometers. **a** the reference interferometer; **b** the testmass-bench measurement interferometer; **c** the testmass-testmass measurement interferometer

(TBMI) measures the relative path-length fluctuations between the simulated testmass (here replaced by a mirror installed on a nanopositioning stage) located on the left side of the optical bench and the optical bench, as shown in Fig. 8b. The testmass-testmass measurement interferometer (TTMI) is sensitive to the relative distance of the two simulated testmasses to each other, as shown in Fig. 8c. Path-length fluctuations of the modulation bench resulting from the environmental noises are measured in each individual interferometer and canceled in the differential phase 'R-M' ('R' and 'M' refer to the reference interferometer and the measurement interferometer, respectively). So, path-length differences before the optical bench are canceled by referring all measurements to the reference interferometer and only those on the optical bench are coupled into the path-length ranging.

## Experimental Results and Discussions

Before evaluating the path-length measurement sensitivity of the prototype, it is necessary to measure the background noise of the laser interferometer prototype and phasemeter. The experimental setup is following: dividing the TTMI's readout from one photodiode into two parts, then adopting the phasemeter to measure the phase difference between them. The data were analyzed with two methods called amplitude spectral density (ASD) and LASD. The Fig. 9a shows that the background noise of the prototype is about 100 pm/$\sqrt{}$Hz within the frequency regime of 1 mHz–1 Hz.

The path-length measurement sensitivity obtained from the TTMI is described by the Fig. 9b, from which can be derived that the path-length measurement sensitivity of the laser interferometer is better than 200 pm/$\sqrt{}$Hz in the frequency band of 10 mHz–1 Hz. Within the lower frequency range of 1 mHz–10 mHz, the noise level increases with decreasing frequency.

Comparing with the sensitivity distribution of the blue and red curves at the lower frequencies in Fig. 9, it can be deduced that the main factor affects the ranging accuracy is the thermal noise resulting from the temperature fluctuation of the surrounding environment. It is because that there is only one air conditioner to adjust the room temperature, and it is the only thermostat. Besides, although the vacuum chamber and invar steel optical bench are adopted, the mounting brackets of all components are made of aluminum, the thermal expansion coefficient of

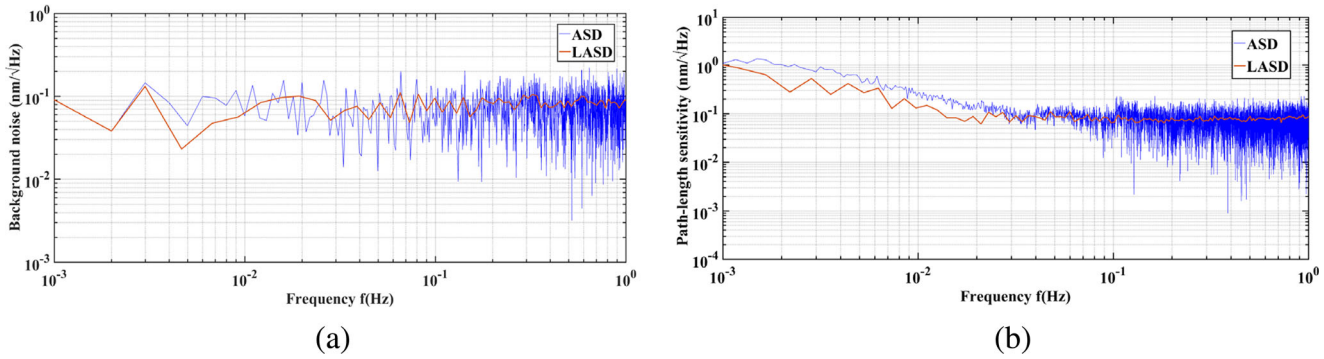


**Fig. 9** Background noise and path-length sensitivity of the TTMI. **a** background noise; **b** path-length sensitivity

which is only about $10^{-5}$/°C, it is the weak point in the current design of the setup. So, the path-length measurement sensitivity of the laser interferometer prototype is better than 200 pm/$\sqrt{\text{Hz}}$ in the frequency range of 10 mHz–1 Hz, but decreasing with a linear function with decreasing frequency within the frequency range of 1 mHz–10 mHz.

Comprehensively considering the possible noises, other noise sources are analyzed as follows (Sheard et al. 2012): (1) laser frequency noise, the relative instability of laser frequency is about $3 \times 10^{-9}$ and the arm length difference is about $5 \times 10^{-3}$ m, so the laser frequency noise is about 15 pm/$\sqrt{\text{Hz}}$; (2) USO noise, the relative frequency instability of USO adopted in AOM is about $10^{-7}$, the central frequency of which is 70 MHz, so the frequency instability is about 7 Hz, which will affect the phase-meter's measurement performance; besides, the frequency and phase noise of USO used in the phase-meter will be directly coupled into the ranging performance; (3) pointing-induced noise, which is caused by the instability of the optical mounts installed on the optical bench, phase changes due to the beam walk effects; (4) spurious electronic phase-shifts, which results from the temperature or stress fluctuations of the cables and the phasemeter's analog front end circuit. Previous investigations showed that it mainly affected the path-length measurement sensitivity in the frequency range of 1 mHz–10 mHz ; (5) parasitic signals noise, which is caused by ghost beams, electrical cross coupling and so on; (6) photo-detector electronic noise, the low signal-to-noise ratio (SNR) of which affects the measurement accuracy of the phasemeter. However, limited by the great background noise of the laser interferometer, how the above noises affect the ranging accuracy can't be quantitatively evaluated under the current condition, but the related experiments and simulations will be carried out.

### Summary

Some results of investigations on an on-ground polarizing laser interferometer prototype used for path-length fluctuations measurement were presented. The results show that the path-length measurement sensitivity of the laboratory prototype meets the requirement of the SAGM mission, but there is still a long way to go for the Taiji mission. Next step, the path-length fluctuations measurement sensitivity of this prototype will be improved for developing an engineering model in the future.

## Methodological Demonstration of Laser Pointing Modulation

In the laser interferometer system, the laser beam pointing jitter noise is expected to be one of the most prominent optical-path noise (Bender 2005). The spacecraft jitter caused by the non-conservative forces, such as atmosphere, solar wind, solar radiation, cosmic rays, etc. can be suppressed by the disturbance reduction system (Schumaker 2003). But the residual attitude dynamics of the spacecraft and the Proof Mass will even result in the jitter of transmitting light. After several hundred kilometers' spreading in SAGM mission or several million kilometers' spreading in Taiji mission, the transmitting light received by local spacecraft is mixed with local laser and the beat-note signal is detected by the photo-detector. The angular jitter of the transmitting light will cause phase noise due to the geometrical distortion of the receiving telescope, as shown in Fig. 10. The apparent phase noise $\delta\varphi$ in the far field can be showed as (Bender 2005):

$$\delta\varphi = \frac{1}{32}\left(\frac{2\pi}{\lambda}\right)^3 d D^2 \theta_{\text{dc}} \delta\theta \tag{1}$$

where $\theta_{\text{dc}}$ is the static offset error in the pointing, $\delta\theta$ is the pointing jitter, $D$ is the diameter of telescope, $d$ is the amplitude of curvature error in the wave-front caused by the geometrical distortion of the receiving telescope and $\lambda$ is the laser wavelength. In the SAGM mission, over one hundred kilometers, the laser beam pointing direction $\theta_{\text{dc}}$ have to be aligned as precise as 20 nrad, and the variation of the alignment $\delta\theta$ should be kept no more than 1 $\mu$ rad/$\sqrt{\text{Hz}}$ at the frequencies from 1 mHz to 1 Hz (Sheard et al. 2012). Otherwise, the beam pointing jitter noise will dominate the displacement noise budget of interferometric measurement system and make the detection of gravity fields impossible. So, to achieve the desired beam pointing stability, an active feed-back control system is essential.

### Design and Architecture

The laser beam pointing control system built by us is composed of laser modulation bench and laser interferometer bench, as shown in Fig. 11. In the laser modulation bench, a 300 mW linear polarized single mode laser with wavelength of 1064 nm is split by a 50:50 beam splitter after passing through the Faraday isolator. Then the two split beams are sent into two AOMs, and the offset frequency between the two AOMs is 1 MHz. One of the laser beams is used to simulate the receiving laser while the other is used as the local laser. The two laser beams are fiber-coupled and sent to the laser interferometer bench. In the laser interferometer bench, a beam reflected by the mirror on the PZT (XMT XS-330.2SL) controlled by so-called P-J-controller is used to simulate beam pointing jitter of the receiving beam. The other PZT (PI s330.2 SL) controlled by P-controller is used for our beam pointing control system to adjust the local beam parallel to the simulated receiving beam. The two beams are interfered at a 50:50 beam-splitter and the relative angle between them is read out by the differential

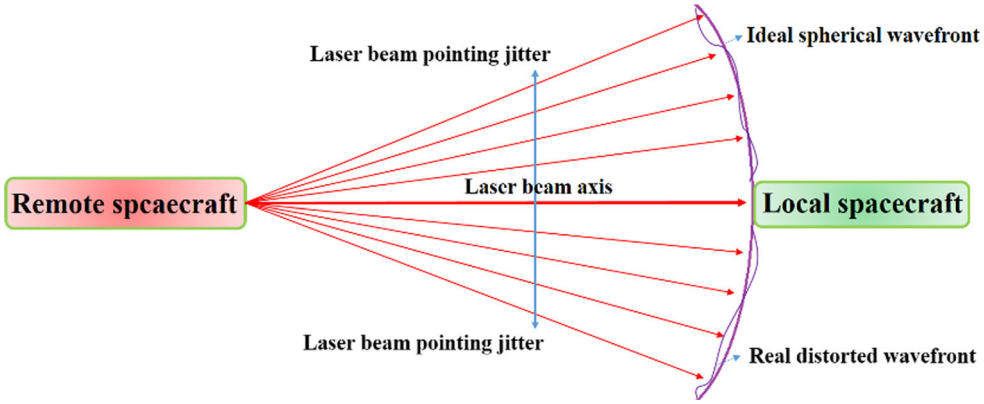


**Fig. 10** Schematic diagram of the laser beam jitter error

wave-front sensing (DWS) technique (Heinzel et al. 2003). Consisting of a quadrant photo detector and a phasemeter, DWS is a well-known technique for measuring the relative wave-front misalignment between two beams with high sensitivity, see Fig. 12 (Sheard et al. 2012).

In small misalignment, the average phase difference $\Delta\theta$ between opposing halves of quadrant photo detector (QPD) can be approximated shown as:

$$\Delta\theta \approx \frac{16r}{3\lambda} \cdot \alpha = k \cdot \alpha \tag{2}$$

where $\alpha$ is the relative wave-front tilt, $r$ is the beam radius, $\lambda$ is the laser wavelength and $k$ is the conversion factor. Acquiring the real-time information of relative angles offered by in-loop readout, the beam pointing controller regulates the PI steering mirror (PI s330.2 SL) which drives the direction of the local laser to follow and lock the direction of the simulated receiving laser to improve the pointing stability. The real-time performance of the beam pointing control system is evaluated by out-of-loop readout.

## Experimental Results and Discussions

During the experiment, the P-J-controller commands on XMT steering mirror to rotate around yaw and pitch axis simultaneously. To simulate the situation of SAGM, the amplitudes

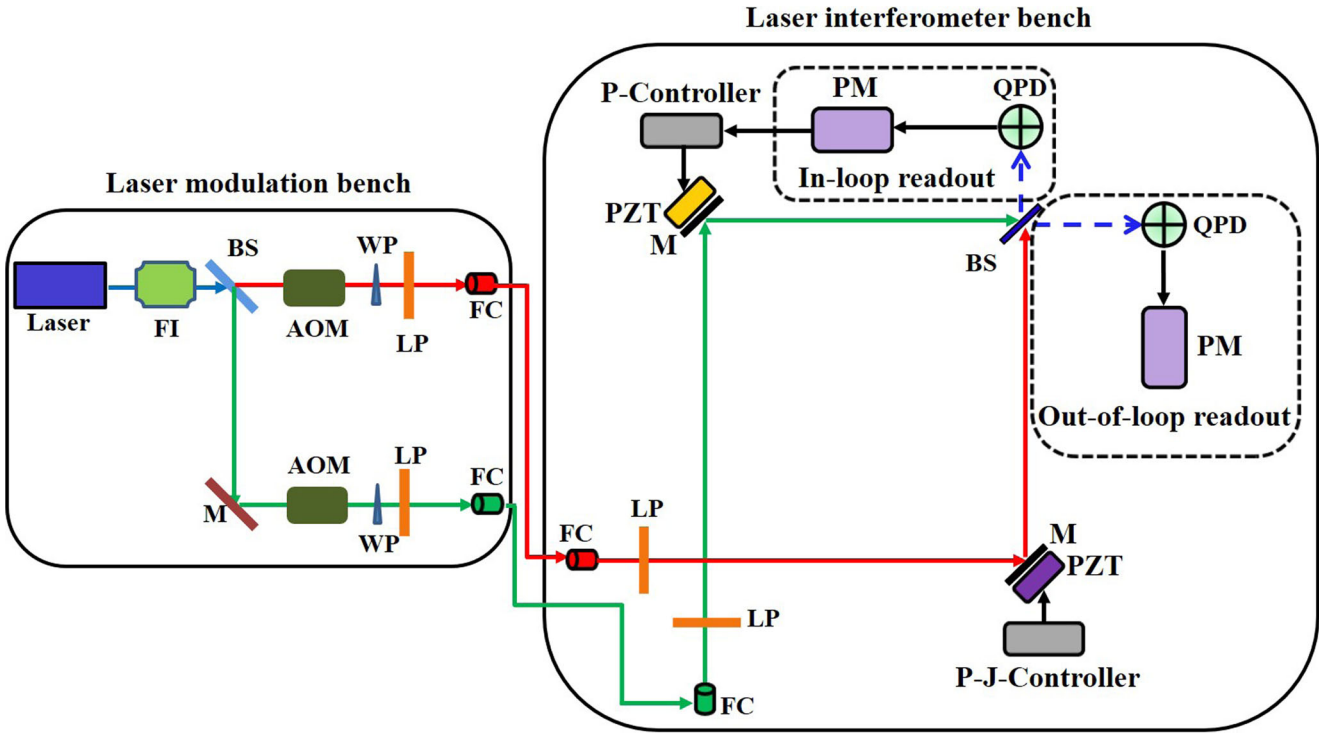


**Fig. 11** Schematic diagram of the beam pointing control system. FI: Faraday isolator, BS: 50:50 Beam Splitter, M: Mirror, AOM: Acousto-optical Modulator, WP: Wedged Plate, LP: Linear Polarizer, FC: Fiber coupler, P-J-Controller: Pointing Jitter Controller, P-Controller: Pointing Controller, PM: Phasemeter, PZT: Piezoelectric Ceramic Transducer, QPD: Quadrant Photo Detector

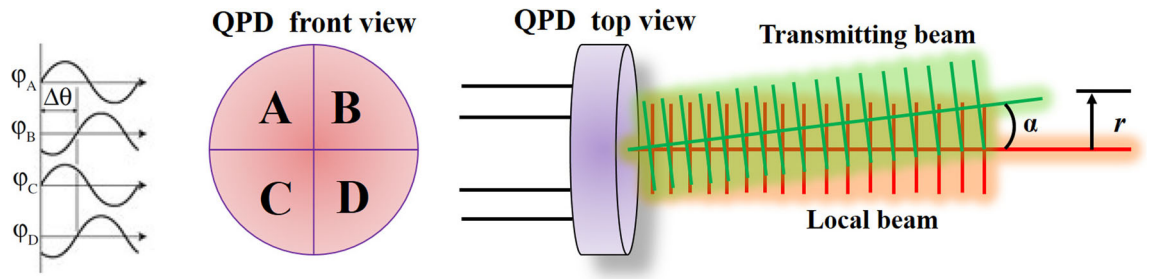


**Fig. 12** Principle of DWS technique

of modulated pointing jitters, both yaw and pitch, are set to 50 $\mu$rad/$\sqrt{\text{Hz}}$. For simplicity, the frequency of simulated jitter is fixed at 10 mHz. The P-controller will drive PI steering mirror to adjust the simulated local laser parallel to the simulated receiving laser in order to compensate the misalignment. The experiment lasts four hours, first two hours is for open loop and last two hours for feedback control. The experimental data shown is analyzed in ASD, see Fig. 13. The blue dotted lines are open loop data, the black dotted lines are in-loop data, the green dots are out-of-loop data and the red solid lines are LASD for out-of-loop data.

After the feedback control turned on, inside the frequency regime of 1 mHz–1 Hz, the residue pointing jitters of yaw and pitch motions are approximately 80 nrad/$\sqrt{\text{Hz}}$ and 90 nrad/$\sqrt{\text{Hz}}$, respectively. Furthermore, the in-loop data shows that this pointing control system has the potential to reach about 1 nrad/$\sqrt{\text{Hz}}$ when the readout noise is suppressed. While the amplitude of the simulated pointing jitter is set to 5 $\mu$rad/$\sqrt{\text{Hz}}$, the stability of the beam pointing direction can be kept better than 10 nrad/$\sqrt{\text{Hz}}$ (Dong et al. 2014).

## Summary

A methodological demonstration of the laser beam pointing control system for the Taiji and SAGM missions has been accomplished. With beam pointing control system turned on, the stability of the beam pointing direction can be kept at 80 nrad/$\sqrt{\text{Hz}}$ and 90 nrad/$\sqrt{\text{Hz}}$ for yaw and pitch direction, respectively In the real situation of the Taiji and SAGM, the received light will be at pW level. Therefore, shot noise dominates and greatly increases the readout noise of DWS system. The SNR will be exceedingly reduced which will make the control of beam pointing more difficult. To build and investigate such a control system for pW received laser beam is the primary task in the following research.

## Methodological Demonstration of Laser Phase-Locking Control

### Design and Architecture

The linearly polarized light emitted from the laser passes through a Faraday isolator to avoid back-reflection of the laser beam. Then, the laser beam is divided into two beams by the BS, and the two beams are modulated by using AOMs at approximately 70 MHz with a frequency difference $f_{\text{het}}$ of 1 MHz, the relative frequency instability of which is $10^{-7}$. After that, the two frequency-shifted beams are separated by two BSs, producing a heterodyne

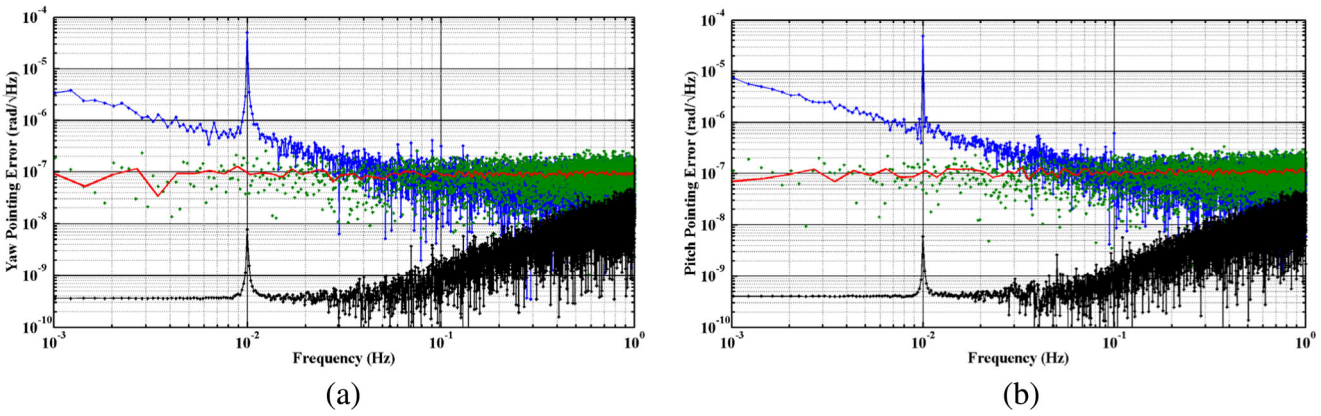


**Fig. 13** **a** Results of rotating around yaw axis before control (blue points) and in control (green points) in the amplitude of 50 $\mu$rad/$\sqrt{\text{Hz}}$; **b** Results of rotating around pitch axis before control (blue points) and in control (green points) in the amplitude of 50 $\mu$rad/$\sqrt{\text{Hz}}$. The red curves present the LASD of yaw motion or pitch motion in out-of-loop; the black dotted lines are in-loop data for yaw and pitch motion

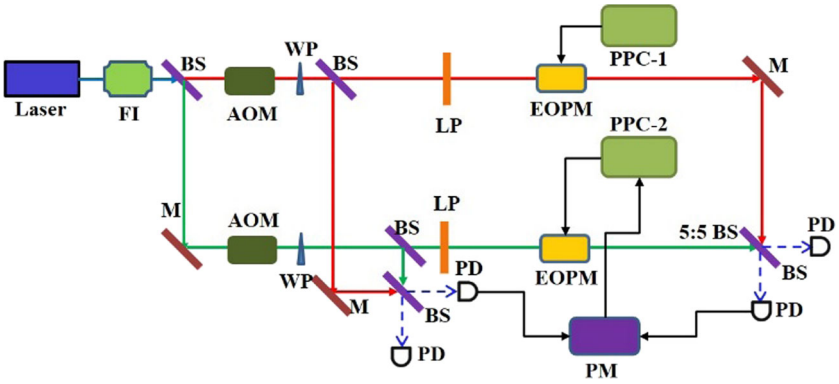


**Fig. 14** Schematic diagram of laser phase-locking control. FI: Faraday Isolator, BS: Beam Splitter, M: Mirror, AOM: Acousto-optic Modulator, WP: Wedged Plate, LP: Linear Polarizer, EOPM: Electro-optic Phase Modulator, PM: Phasemeter, PPC: Programmable Power Controller, PD: Photo detector

interference signal at another BS, which is called reference interferometer. The LP (Linear Polarizer) is to make the light become a pure "s" polarized light for reducing the EOPM's (Thorlabs EO-PM-NR-C2, the phase modulation coefficient is about 11.37 mrad/V@1064 nm during the voltage range of 0 V–100 V) voltage-phase error. Similarly, the two beams after passing through the EOPMs form another interferometer, which is called measurement interferometer. Here, two EOPMs, two programmable power controllers, a phasemeter, a reference interferometer and a measurement interferometer constitute a methodological demonstration of laser phase-locking control system (Fig. 14).

## Experimental Results and Discussions

The process of laser phase-locking control will be depicted in the following. For the halfwave voltage of the EOPM is 240 V, to simulate the phase change of the interference signal, the output voltage of PPC-1 is set as follows:

$$V = 2.4Cos(0.002\pi t + \Delta\varphi)V \tag{3}$$

This voltage is used to drive the EOPM to change the phase of the red laser beam, so a phase difference will be formed between the reference interferometer and the measurement interferometer. The phase difference measured by the phasemeter is fed back to the PPC-2 to control the other EOPM to change the phase of the green laser beam, which will make the phase change of the green laser beam tracking that of the red laser beam.

For the experimental system is installed on an aluminum optical bench, the temperature fluctuation noise is the main noise here. The phase difference resulting from the voltage change of PPC-1 will be submerged in the thermal noise. So, here the thermal noise of the interferometer is used

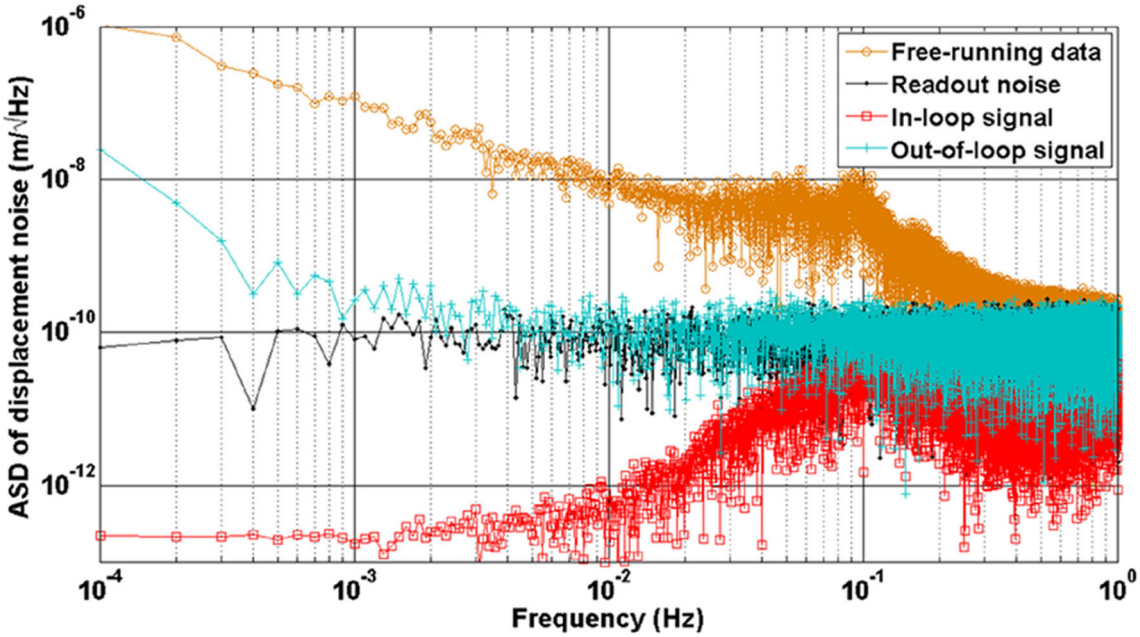


**Fig. 15** Results of laser phase-locking

as the simulated signal, the phase of which is tracked and locked by the PM, PPC-2 and EOPM. The experiment lasts four hours, during the first 2 h, keeping the environmental conditions as stable as possible and the control loop is shut down, and recording the phase data resulting from the path-length fluctuation between the reference interferometer and the measurement interferometer; during the last 2 h, the environmental conditions are set the same as the first 2 h, but opening the control loop to make the phase change tracking with the path-length fluctuation of the interferometer, then also recording the phase data. Then the data are compared to evaluate the performance of the laser phase-locking control. Here, the beat frequency is 1 MHz, and the power of the slave laser and the master laser are about 100 $\mu$W.

The results of laser phase-locking control are shown in Fig. 15. Limited by the readout noise and optical pathlength noise, the phase lock loop is working at nanometer level. It could be seen that the phase difference between the slave laser and the master laser is suppressed from $10^{-7}$ to $3 \times 10^{-10}$ m/ $\sqrt{}$Hz at 1 mHz after the phase locking loop is turned on. This directly demonstrates the functionality of our control scheme.

### Summary

A methodological demonstration of laser phase-locking control system has been established, which proves the validity of the scheme of phase-locking. But in the Taiji or SAGM mission, the receiving light will be pW, the shot noise dominates and greatly increases the readout noise of the phase measurement system. Therefore, how to solve the problem of weak light detection is the primary task in the future

## Conclusions

The development of laser interferometer prototype used for satellite-to-satellite ranging has been presented in this paper. Experimental demonstrations of the basic concept and principle are in progress and further detailed analysis is ongoing. This interferometer prototype is intended to demonstrate the feasibility of some key techniques embedded in space laser interferometer. But all the results are just the beginning of efforts in China toward detecting gravitational waves and mapping the Earth's gravity field. There are still many key techniques to be solved, such as weak light detection, relative time and frequency alignment, etc. Next step, using hydroxy-catalysis or other surface bonding techniques to fix the optics on an ultra-stable glass-ceramic baseplate made of Clearceram or Zerodur and lowering the pressure of the vacuum chamber to further reduce the thermal noise is being planned. Besides, adopting another nano-positioning stage to drive the mirror located on the right side of the optical bench to simulate a displacement caused by the orbit drift, and using the existing nano-positioning stage on the left side to simulate the science signals resulting from gravity variations of the planet is the primary task in our future work, in considering how to identify and extract the science signal from the Doppler shift between the two spacecraft. In addition, other key techniques embedded in space laser interferometer for Taiji mission such as arm-locking, time delay interferometer, laser communication, absolute distance measurement, etc. are under consideration.

**Acknowledgements** This work was supported by the Strategic Priority Research Program of the Chinese Academy of Sciences, Grant No. XDB23030200, and the National Natural Science Foundation of China, Grant No. 61575209.

## References

Abbott, B.P., Abbott, R., Abbott, T.D., et al.: GW151226: Observation of gravitational waves from a 22-solar-mass binary black hole coalescence. Phys. Rev. Lett. **116**(24), 241103 (2016a)

Abbott, B.P., Abbott, R., Abbott, T.D., et al.: Observation of gravitational waves from a binary black hole merger. Phys. Rev. Lett. **116**(6), 061102 (2016b)

Abbott, B.P., Abbott, R., Abbott, T.D., et al.: GW170104: observation of a 50-solar-mass binary black hole coalescence at Redshift 0.2. arXiv:1706.01812 (2017)

Bender, P.L.: Wavefront distortion and beam pointing for LISA. Class. Quantum Grav. **22**(10), S339–S346 (2005)

Bender, P.L., Nerem, R.S., Wahr, J.M.: Possible future use of laser gravity gradiometers. In: Earth Gravity Field from Space—from Sensors to Earth Sciences, pp. 385–392. Springer, Netherlands (2003)

Bender, P.L., Begelman, M.C., Gair, J.R.: Possible LISA follow-on mission scientific objectives. Class. Quantum Grav. **30**(16), 165017 (2013)

Bykov, I., Delgado, J.J.E., Marín, A.F.G., Heinzel, G., Danzmann, K.: LISA phasemeter development: Advanced prototyping. J. Phys.: Conf. Ser. **154**(1), 012017 (2009)

Cyranoski, D.: Chinese gravitational-wave hunt hits crunch time. Nature **531**, 150–151 (2016)

Danzmann, K., LISA Study Team: LISA: laser interferometer space antenna for gravitational wave measurements. Class. Quantum Grav. **13**(11A), A247–A250 (1996)

Dehne, M., Cervantes, F.G., Sheard, B., Heinzel, G., Danzmann, K.: Laser interferometer for spaceborne mapping of the Earth's gravity field. J. Phys.: Conf. Ser. **154**(1), 012023 (2009)

Dong, Y.H., Liu, H.S., Luo, Z.R., Li, Y.Q., Jin, G.: Methodological demonstration of laser beam pointing control for space gravitational wave detection missions. Rev. Sci. Instrum. **85**(7), 074501 (2014)

Gerberding, O., Sheard, B., Bykov, I., Kullmann, J., Delgado, J.J.E., Danzmann, K., Heinzel, G.: Phasemeter core for intersatellite laser heterodyne interferometry: modelling, simulations and experiments. Class. Quantum Grav. **30**(23), 235029 (2013)

Gong, X., Xu, S., Bai, S., Cao, Z., Chen, G., Chen, Y., He, X., Heinzel, G., Lau, Y.K., Liu, C., Luo, J., Luo, Z., Patón, A.P., Rüdiger, A., Shao, M., Spurzem, R., Wang, Y., Xu, P., Yeh, H.C., Yuan, Y.,

Zhou, Z.: A scientific case study of an advanced LISA mission. Class. Quantum Grav. **28**(9), 094012 (2011)

Heinzel, G.: Satellite interferometry from LTP and GRACE Follow-On to LISA. In: International Symposium on Gravitational Waves. University of Chinese Academy of Sciences, Beijing (2017)

Heinzel, G., Braxmaier, C., Schilling, R., Rüdiger, A., Robertson, D., Te Plate, M., Wand, V., Arai, K., Johann, U., Danzmann, K.: Interferometry for the LISA technology package (LTP) aboard SMART-2. Class. Quantum Grav. **20**(10), S153–S161 (2003)

Heinzel, G., Wand, V., Garcia, A., Jennrich, O., Braxmaier, C., Robertson, D., Middleton, K., Hoyland, D., Rüdiger, A., Schilling, R., Johann, U., Danzmann, K.: The LTP interferometer and phasemeter. Class. Quantum Grav. **21**(5), S581 (2004)

Heinzel, G., Braxmaier, C., Danzmann, K., Gath, P., Hough, J., Jennrich, O., Johann, U., Rüdiger, A., Sallusti, M., Schulte, H.: LISA interferometry: recent developments. Class. Quantum Grav. **23**(8), S119 (2006)

Lhermite, J., Desfarges-Berthelemot, A., Kermene, V., Barthelemy, A.: Passive phase locking of an array of four fiber amplifiers by an all-optical feedback loop. Opt. Lett. **32**(13), 1842–1844 (2007)

Li, Y.Q., Luo, Z.R., Liu, H.S., Dong, Y.H., Jin, G.: Laser interferometer used for satellite–satellite tracking: an on-ground methodological demonstration. Chin. Phys. Lett. **29**(7), 079501 (2012)

Liang, Y.R., Duan, H.Z., Yeh, H.C., Luo, J.: Fundamental limits on the digital phase measurement method based on cross-correlation analysis. Rev. Sci. Instrum. **83**(9), 095110 (2012)

Liu, H.S., Dong, Y.H., Li, Y.Q., Luo, Z.R., Jin, G.: The evaluation of phasemeter prototype performance for the space gravitational waves detection. Rev. Sci. Instrum. **85**(2), 024503 (2014)

Nagano, S., Yoshino, T., Kunimori, H., Hosokawa, M., Kawamura, S., Sato, T., Ohkawa, M.: Displacement measuring technique for satellite-to-satellite laser interferometer to determine Earth's gravity field. Meas. Sci. Technol. **15**(12), 2406–2411 (2004)

Nagano, S., Hosokawa, M., Kunimori, H., Yoshino, T., Kawamura, S., Ohkawa, M., Sato, T.: Development of a simulator of a satellite-to-satellite interferometer for determination of the Earth's gravity field. Rev. Sci. Instrum. **76**(12), 124501 (2005)

Olivier, C., Christian, S., Luca, M., Roger, H., Pierluigi, S.: A spaceborne gravity gradiometer concept based on cold atom interferometers for measuring Earth's gravity field. Microgravity Sci. Technol. **26**(3), 139–145 (2014)

Pierce, R., Leitch, J., Stephens, M., Bender, P., Nerem, R.: Intersatellite range monitoring using optical interferometry. Appl. Opt. **47**(27), 5007–5019 (2008)

Sascha, K., Christian, V., Andreas, R., et al.: Miniaturized lab system for future cold atom experiments in microgravity. Microgravity Sci. Technol. **29**(1–2), 37–48 (2017)

Schumaker, B.L.: Disturbance reduction requirements for LISA. Class. Quantum Grav. **20**(10), S239–S253 (2003)

Shaddock, D., Ware, B., Halverson, P.G., Spero, R.E., Klipstein, B.: Overview of the LISA Phasemeter. J. Phys.: Conf. Ser. **873**(1), 654–660 (2006)

Sheard, B.S., Heinzel, G., Danzmann, K., Shaddock, D.A., Klipstein, W.M., Folkner, W.M.: Intersatellite laser ranging instrument for the GRACE follow-on mission. J. Geodyn. **86**(12), 1083–1095 (2012)

Yeh, H.C., Yan, Q.Z., Liang, Y.R., Wang, Y., Luo, J.: Intersatellite laser ranging with homodyne optical phase locking for Space Advanced Gravity Measurements mission. Rev. Sci. Instrum. **82**(4), 044501 (2011)